processes

MDPI

Article

Research on High-Temperature Resistant Bridging Composite Cement Slurry Technology for Deep Well Loss Circulation Control

Biao Ma [1,*], Kun Zheng [1], Bin Feng [1], Qing Shi [1], Lei Pu [2,*], Chengjin Zhang [1], Zhengguo Zhao [3], Shengbin Zeng [2] and Peng Xu [2]

[1] Downhole Service Company of CNPC Chuanqing Drilling Engineering Company Limited, Chengdu 610052, China; zhenk_jx@cnpc.com.cn (K.Z.); fengb02@cnpc.com.cn (B.F.); shiq_jx@cnpc.com.cn (Q.S.)
[2] Hubei Key Laboratory of Oil and Gas Drilling and Production Engineering, Yangtze University, Wuhan 430100, China; shengbinzeng2025@163.com (S.Z.); cdxupeng@yangtzeu.edu.cn (P.X.)
[3] Drilling Fluid Company of CNPC Chuanqing Drilling Engineering Company Limited, Chengdu 610052, China; zhaozhengguo_sc@cnpc.com.cn
* Correspondence: mabiao_scjx@cnpc.com.cn (B.M.); leipu@yangtzeu.edu.cn (L.P.)

Abstract

Circulation is one of the most prevalent and severe complications during the drilling and completion of deep and ultra-deep wells, especially in fractured and karstic formations. In regions such as the Sichuan Basin, bottom-hole temperatures exceeding 200 °C, limited formation strength, and frequent lithological alternations significantly reduce the effectiveness of conventional granular materials under high-temperature and long open-hole conditions. Bridging-type plugging systems based on particle gradation or principles often exhibit low success rates due to fiber softening, rubber aging, and erosion-induced deterioration of the sealing structure. In this study, a high-temperature-resistant bridging composite system was developed to meet the extreme conditions in deep and ultra-deep wells. By incorporating temperature-resistant bridging particles and flexible reinforcing components, the slurry establishes a synergistic "bridging–filling–densification" sealing mechanism. Meanwhile, the combined use of retarders, fluid-loss reducers, and rheology modifiers ensures stable pumpability and adequate curing densification at 200 °C. Overall, the results provide new insights and experimental evidence for the design of high-temperature cement-based plugging materials, offering a promising approach for improving loss-control effectiveness and wellbore strengthening in complex intervals.

Keywords: deep well; severe loss circulation; high temperature; cement slurry; composite plugging

Check for updates

Academic Editor: Guining Lu

Received: 18 November 2025
Revised: 12 January 2026
Accepted: 14 January 2026
Published: 20 January 2026

Copyright: © 2026 by the authors. Licensee MDPI, Basel, Switzerland. This article is an open access article distributed under the terms and conditions of the Creative Commons Attribution (CC BY) license.

1. Introduction

Loss circulation is widely recognized as one of the most critical downhole complications during the drilling and cementing of deep and ultra-deep wells, particularly in fractured and vuggy formations [1–3]. As oil and gas exploration in China continues to extend toward deeper and more structurally complex formations, long open-hole intervals have become increasingly common, significantly increasing the risk of severe loss circulation and deterioration of wellbore integrity [4–6].

Deep formations in regions such as the Sichuan Basin are characterized by the coexistence of high temperatures, complex fracture–vug systems, and abnormal pressure condi-

tions, where wellbore instability and loss circulation frequently occur simultaneously [7]. Field statistics indicate that the success rate of loss-circulation control in deep formations remains below 40%, resulting in substantial increases in non-productive time and drilling costs, and posing serious constraints on exploration and development efficiency [8,9].

Existing loss-prevention and control approaches are mainly based on rock-mechanics theories, such as and fracture-closure concepts [10], or empirical particle-bridging criteria, including 2/3 bridging and D50 filling rules [11–13]. Although these methods are effective in conventional wells, their performance in deep, high-temperature, and long open-hole sections is limited, with frequent recurrence of loss events [14]. The primary reasons include the thermal degradation of fibers and elastic particles [15,16], as well as strong erosion, high stress fluctuations, and large loss channels that undermine the stability of plugging structures [17].

A representative case from a deep well in the Sichuan Basin further illustrates the challenges associated with recurrent loss circulation in complex formations. During drilling of the second section of the Huangliu Formation, multiple severe loss events were encountered. Initial treatment using a sealing drilling fluid involved an injection volume of 8 m^3, which reduced the loss rate to approximately 11 m^3/h but failed to achieve complete sealing. Subsequent operations increased the circulation rate to 360 L/min, resulting in a reservoir fluid reduction of 3.1 m^3, while the loss rate remained nearly unchanged. During the second and third treatment cycles, a total of 24 m^3 was injected, with a maximum squeezing pressure of 1270 psi, yet the loss rate persisted at around 10 m^3/h. After a subsequent logging operation, throttled circulation was performed at the bottom hole, during which the pump pressure dropped from 790 psi to 500 psi, followed by renewed total loss. The cumulative loss volume reached approximately 80 m^3, with a peak loss rate of about 35 m^3/h. In the fourth treatment cycle, only 6 m^3 was injected at a maximum squeezing pressure of approximately 500 psi, which failed to establish effective sealing, ultimately leading to well abandonment. This case highlights that in deep and complex formations, conventional particulate bridging materials often fail to penetrate intricate loss pathways and form dense plugging structures. Moreover, under high-temperature and high-pressure conditions, plugging materials are prone to thermal aging and mechanical degradation, which can induce secondary loss circulation after temporary plugging.

Compared with particulate loss-control materials, cement-based systems can penetrate loss channels and solidify into an integral structure, making them an important option for deep loss-circulation control [18,19]. Previous studies have attempted to enhance cement retention and load-bearing performance through the incorporation of particles, flakes, and fibers [20–22]. However, conventional cement loss-control systems still suffer from poor high-temperature stability, rheological uncontrollability, and difficulty in forming durable plugging structures under extreme conditions.

Therefore, the primary objective of this study is to develop a high-temperature-resistant composite system suitable for deep and ultra-deep wells. The proposed system aims to maintain controllable rheological properties at elevated temperatures, achieve effective fracture plugging through synergistic bridging and filling mechanisms, and sustain long-term integrity under high differential pressure and erosive conditions, thereby improving loss-circulation control efficiency and overall wellbore quality in deep complex formations.

2. Design Methodology for Bridging Composite Cement Slurry

In fractured loss-circulation formations, conventional cement plugging systems are prone to failure under high-temperature conditions due to material aging, uncontrolled thickening, and unstable plugging structures. Elevated temperatures can induce thermal

aging or softening of bridging materials such as fibers and elastic particles, thereby destabilizing the bridging structures within fractures [23–25]. Under cyclic pressure differentials, the plugging layer can be compromised, making it difficult for the cement slurry to remain effectively in place. Additionally, cement systems at high temperatures often exhibit shortened thickening times, reduced fluidity, and diminished cementstone strength, thereby reducing the durability of the plugging effect [26].

To address these mechanisms, this study proposes a high-temperature-resistant bridging composite design. By incorporating high-temperature-resistant additives, precise control over the cement slurry's thickening time, rheological properties, and water–cement ratio can be achieved, ensuring pumpability and operability under high-temperature and high-pressure conditions. Colloidal stabilizing materials are incorporated to maintain the slurry's structural integrity and prevent water separation and stratification. High-temperature-resistant toughening particles are used to construct the bridging framework, and high-stability filling particles are added to enhance the plugging layer's density and pressure-bearing capacity. Additionally, temperature-resistant fibers are incorporated to reinforce the structural integrity and sealing performance of the cured cement stone [27].

Through the synergistic integration of additive regulation, colloidal stabilization, particle bridging, and fiber reinforcement, a bridging composite system with controllable rheology, structural stability, and long-term plugging capability is developed. The working mechanism of this system is illustrated in Figure 1. This system enables efficient placement, effective retention, and stable curing of cement slurry in fractured loss-circulation formations, providing a novel material-design approach for loss-circulation management.

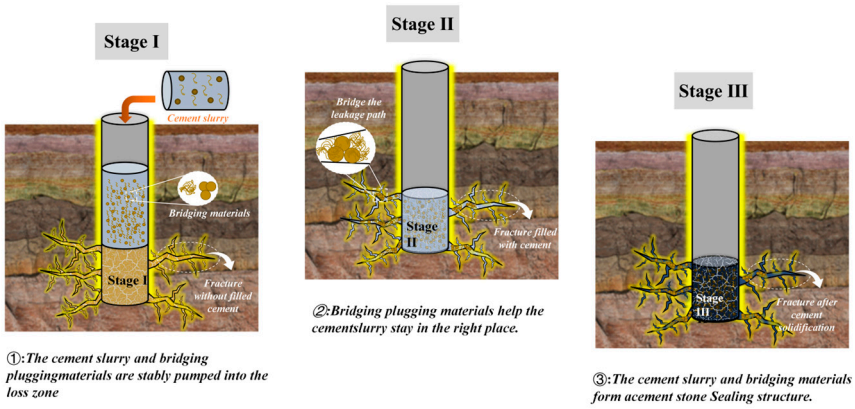


Figure 1. Schematic Diagram of Cement Slurry-Bridging Plugging Material Composite Sealing System.

3. Materials and Methods

3.1. Experimental Materials and Formulation

The cement utilized in this study was Class G oil-well cement produced by JiaHua Company (Jingzhou, China), with ordinary tap water being used for sample preparation. Nano-silica was supplied by Shanghai XiaoChao Nano Technology Co., Ltd. (Shanghai, China); carbon fiber was provided by Carbonene Technology (Shenzhen) Co., Ltd. (Shenzhen, China); the dispersant was obtained from Guangzhou Dingzun Trading Co., Ltd. (Guangzhou, China); the suspension stabilizer and retarder were sourced from Shanxi Feike New Material Technology Co., Ltd. (Shanxi, China); microsilica was supplied by Henan Zhuangwei New Material Co., Ltd. (Henan, China); silica fume was provided by Nangong Zhongmai Metal Material Co., Ltd. (Nangong, China).; the fluid-loss additive was obtained from Jieyang New Material Co., Ltd. (Jieyang, China); and the defoamer was supplied by Shenzhen Baoqingcheng Trading Co., Ltd. (Shenzhen, China). The high-temperature plugging particles were synthesized in-house in our laboratory for evaluating the plug-

ging performance of the bridging composite cement slurry in simulated high-temperature fractured loss-circulation formations.

The composite bridging cement slurry consists of cement, silica flour, microsilica, fluid-loss reducer, retarder, dispersant, defoamer, suspension stabilizer, nano-SiO_2, temperature-resistant fibers, and plugging particles. The base formulation is composed of 100 wt% cement, 35 wt% silica flour, 4 wt% microsilica, 4 wt% fluid-loss reducer, 3 wt% retarder, 1.8 wt% dispersant, 0.5 wt% defoamer, 0.5 wt% suspension stabilizer, 1 wt% nano-SiO2, and 0.5 wt% carbon fiber. The lost-circulation plugging experimental apparatus is shown in Figure 2. The dosage of plugging particles is adjusted according to fracture width and particle-size distribution to ensure effective bridging and filling under different fracture conditions.

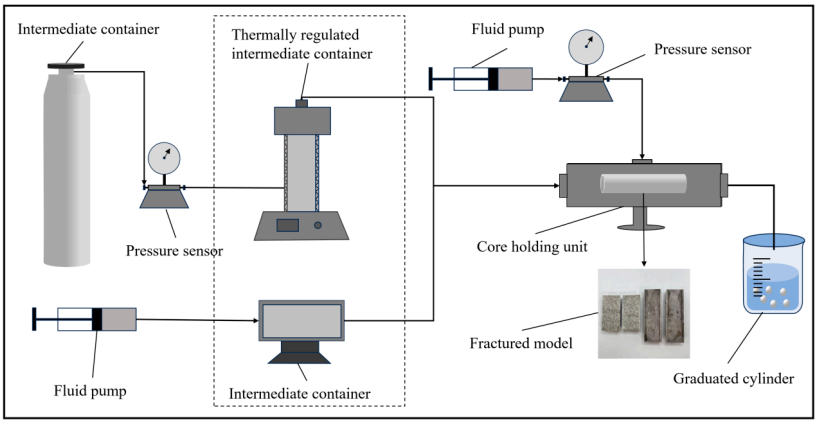


Figure 2. Schematic Diagram of High-Temperature and High-Pressure Fracture Sealing Apparatus.

The instruments utilized are delineated in Table 1 below.

Table 1. Principal Experimental Instruments and Equipment.

Name	Model	Manufacturer/Origin
Constant Speed Stirrer	TG-3060A	Jiangsu Tianguang Instrument Co., Ltd. (Jiangyin, China).
Rotational Viscometer	ZNN-D6	Qingdao Reid Petroleum Instrument Manufacturing Co., Ltd. (Qingdao, China).
High Temperature and High Pressure Thickening Tester	TG-8040DA	Shenyang Tiger Petroleum Instrument Equipment Manufacturing Co., Ltd. (Shenyang, China).
High Temperature and High Pressure Fluid Loss Tester	OFITE-170	OFITE (Houston, TX, USA)
Constant Temperature Water Bath	HH-80	Shanghai Jinghong Laboratory Equipment Co., Ltd. (Shanghai, China).
High Temperature Curing Autoclave	TG-7370D	Jiangsu Tianguang Instrument Co., Ltd. (Jiangyin, China).
Universal Material Testing Machine	HY-20080	Shanghai Hengyi Instrument Co., Ltd. (Shanghai, China).
High Temperature and High Pressure Fracture Plugging Tester	—	Laboratory Self-made
Field Emission Scanning Electron Microscope	SU8010	Hitachi (Tokyo, Japan)
X-ray Diffractometer	Empyrean	PANalytical (Almelo, The Netherlands)
High-temperature roller	XGRL-4A	Qingdao Chuangmeng Instrument Co., Ltd. (Qingdao, China).

3.2. Testing Methodology for Leak-Stopping Cement Slurry

3.2.1. Rheological Properties and Flowability Testing of Cement Slurry

(1) Fluidity Test

The fluidity test of the cement paste was conducted in accordance with the Test Methods for Uniformity of Concrete Admixtures (GB/T 8077-2012) [28], using the truncated-conical mold method. The mold had an upper diameter of 36 mm, a lower diameter of 60 mm, and a height of 60 mm. The experiment was performed at an ambient temperature of (20 ± 2) °C. The testing procedure was as follows: a smooth glass plate was placed horizontally, and the truncated-conical mold was positioned at its center. The uniformly mixed cement paste was poured into the mold, and the surface was leveled using a trowel. Upon vertically lifting the mold, timing was initiated immediately. After the paste had flowed freely on the glass plate for 30 s, the maximum spread diameters in two mutually perpendicular directions were measured, and their average was recorded as the fluidity, thereby describing the differences in flowability among the paste formulations.

(2) High-Temperature and High-Pressure Rheological Property Testing

The rheological properties of the cement slurry were tested in accordance with the Test Methods for Oil Well Cements (GB/T 19139-2012) [29]. Initially, at ambient temperature, the apparent viscosity, plastic viscosity (PV), yield point (YP), and thixotropic properties were measured using a ZNN-D6 six-speed rotational viscometer. The procedure for testing rheological properties under high-temperature and high-pressure conditions was as follows: the prepared cement slurry was placed in a high-temperature consistometer and cured for 1 h under the specified temperature and pressure; it was then cooled to approximately 90 °C, depressurized, removed, and its rheological parameters were subsequently measured using a viscometer at 90 °C under atmospheric pressure.

3.2.2. Cement Slurry Thickening Performance Test

The thickening properties of the cement slurry are used to evaluate its flow-retention and setting characteristics under high-temperature and high-pressure conditions. The experiment was conducted using a TG-8040DA pressurized consistometer manufactured by Shenyang Tiger Petroleum Instrument Equipment Co., Ltd. The prepared cement slurry was poured into the slurry cup, gently vibrated to remove air bubbles, and the bottom cover was securely tightened before it was placed into the consistometer. The temperature and pressure were increased according to the preset program to 180 °C and 50 MPa, respectively, and were maintained for 90 min. The instrument automatically recorded the changes in Consistency Units (CU) over time. According to the Test Methods for Oil Well Cement (GB/T 19139-2012), a consistency of 30 Bc indicates loss of pumpability, whereas 100 Bc represents initial setting [30]. By analyzing the thickening curve, the thickening time and high-temperature stability can be determined, which are used to evaluate the system's high-temperature resistance and construction adaptability.

3.2.3. Colloidal Stability Testing of Cement Slurry

To evaluate the colloidal stability of the cement paste under static conditions, the uniformly mixed paste was poured into a 100mL graduated cylinder and was allowed to stand at room temperature for observation. The presence of clear liquid stratification or changes in the solid–liquid interface in the upper layer was recorded, and the percentage of bleeding water relative to the total paste volume was measured to characterize the system's colloidal stability. Additionally, by comparing the bleeding behavior of pastes treated with different admixtures, the effects of various treatment agents on the structural stability of the colloidal system were evaluated. The system was considered to exhibit good

colloidal stability when no significant stratification or bleeding was observed during the standing period.

3.2.4. Assessment of the Suspension Stability of Plugging Materials

To investigate the suspension performance of lost-circulation materials in cement slurry, the slurry containing lost-circulation particles was placed in grease-coated tubes. All tubes were tapped to eliminate air bubbles and were then placed in a water-curing container at 90 °C in accordance with the Test Methods for Oil Well Cement (GB/T 19139-2012) [29]. Each slurry was cured for 24 h, with water heating turned off 1 h 45 min before removal. After extraction, the tubes were cooled in water for 5 min.

Following cooling, the cementstone specimens were removed and their lengths were measured. Each specimen was then divided into four equal segments, and the volume of each segment was calculated. Each segment was placed on a balance to determine its mass, and its density was calculated using Formula (1).

$$\rho_i = \frac{M_i}{V_i} \tag{1}$$

where:

ρ_i is the density of the ith cementstone segment (g/cm^3);
M_i is the mass of the ith cementstone segment (g);
V_i is the volume of the ith cementstone segment (cm^3).

Prior to curing, the density of the cement slurry was measured. The density difference between the cement slurry and the cementstone specimen was calculated using Formula (2):

$$\frac{\Delta\rho_i}{\rho_s} = \frac{\rho_i - \rho_s}{\rho_s} \times 100 \tag{2}$$

where:

$\Delta\rho_i/\rho_s$ is the density difference of the ith cementstone segment (%);
ρ_i is the density of the ith cementstone segment (g/cm^3);
ρ_s is the density of the cement slurry (g/cm^3).

3.2.5. High-Temperature Fracture Sealing Performance Evaluation

To systematically evaluate the plugging behavior and durability of bridging composite cement slurries in high-temperature fractured formations, a self-developed high-temperature and high-pressure dynamic plugging apparatus was employed for staged testing.

(1) Plugging Formation Performance Test

The plugging cement slurry was placed in a container equipped with a heating device and was heated to 180 °C. The slurry was then injected into a wedge-shaped fracture plate with crack widths of 2–5 mm to assess its bridging and plugging capabilities. The pressure was increased incrementally by 0.25 MPa, with each level maintained for 3 min. The leakage volume and final pressure-bearing capacity were recorded to determine the initial plugging effectiveness.

(2) Post-Curing Pressure-Bearing Performance Test

After plugging completion, the fracture plate was allowed to cure at room temperature for 24 h. The test was then repeated using pure cement slurry as the medium, employing the same incremental pressurization method (0.25 MPa/3 min) until leakage occurred. The critical pressure was recorded to evaluate the pressure-bearing capacity and mechanical stability of the cured plugging layer.

(3) Sealing Performance Test

To investigate the compactness and sealing performance of the plugging layer, the plugged sample was placed in an XGRL-4A high-temperature roller heating furnace and aged at 180 °C for 24 h. After cooling, a stepwise pressurization test (0.25 MPa/3 min) was conducted again using water as the medium in the dynamic plugging apparatus. The pressure at which leakage occurred was recorded to assess the sealing integrity of the plugging layer.

(4) Post-High-Temperature Aging Pressure-Bearing Performance Test

To examine the pressure-bearing performance of the plugging layer under high-temperature formation conditions, the plugged sample was placed in the XGRL-4A high-temperature roller heating furnace and aged at 180 °C for 24 h after plugging completion. Pure cement slurry was then used as the test medium. The test procedure was identical to the previous steps, with incremental pressurization at 0.25 MPa until leakage occurred. The ultimate pressure-bearing capacity of the aged plugging layer was determined to characterize its thermal stability and long-term plugging performance [31].

3.2.6. Mechanical Property Testing of Cementitious Stone Specimens

To evaluate the mechanical properties of the bridging composite cement stone, the prepared slurry was injected into copper cubic molds with a side length of 50.8 mm. The molds were then sealed and placed in a high-temperature curing autoclave, where they were cured at 180 °C for 24 h. After curing, the molds were removed, demolded, and allowed to cool to room temperature.

The compressive strength and elastic modulus of the specimens were tested using a HY-20080 microcomputer-controlled electronic universal testing machine (Shanghai Hengyi Precision Instrument Co., Ltd., Shanghai, China). The loading rate was set at 0.4 kN/s. Each group of specimens was tested three times, and the average value was taken as the compressive strength and elastic modulus of the cementstone formulation.

3.2.7. SEM Characterization of CementStone Microstructure

Microstructural analysis was performed on cement stone specimens cured at 180 °C for 24 h. After curing, the specimens were removed, crushed, and flat surface fragments were selected as SEM samples. To terminate hydration, the samples were immersed in 97% ethanol for 24 h and subsequently dried in an oven at 60 °C for 12 h. After cooling, the samples were mounted on conductive stubs and examined using a field-emission scanning electron microscope (SU8010, Hitachi, Japan) to observe their microstructural features.

3.2.8. Bond Strength Test of Set Cement

To evaluate the interfacial bonding performance of the lost-circulation cement with steel, a custom push-out shear mold was employed. The mold was fabricated from N80 steel (to approximate casing metallurgy) with an inner diameter of 50 mm, outer diameter of 100 mm, and height of 100 mm. The prepared slurry was cast into the mold bore and cured under specified temperature–pressure conditions and curing age to form a cylindrical plug bonded to the steel wall. Tests were conducted on a universal testing machine in displacement control at a constant loading rate; the peak load Fmax (N) was recorded at the moment the set cement cylinder was expelled along the steel–cement interface.

The interfacial shear bond strength was calculated as

$$F_b = \frac{P_b}{\pi d h} \quad (3)$$

where F_b is the interfacial shear bond strength (MPa), d is the mold inner diameter (mm), and h is the bonded height (mm). This approach converts the ultimate push-out load to shear stress via the geometrically defined shear area and is suitable for comparing the bonding capacity of different plugging-cement formulations.

3.2.9. X-Ray Diffraction (XRD) Test of Set Cement

Set-cement phase assemblage and hydration state were characterized by X-ray diffraction (XRD). Specimens were cured at prescribed temperature/pressure, low-temperature dried to constant mass, ground to pass a 75 μm sieve, packed into a low-background holder, and gently pressed. Measurements used Cu Kα radiation (λ = 1.5406 Å) at 40 kV/40 mA over 2θ = 5–70°, step size 0.02°, counting time 1–2 s per step. Silicon was employed as an internal/external standard to calibrate peak positions. Raw patterns underwent background subtraction, peak profile fitting, and Rietveld refinement to obtain semi-quantitative/quantitative contents of clinker phases (C_3S, C_2S), hydration products portlandite, $Ca(OH)_2$; ettringite, AFt, and supplementary constituents, lost-circulation materials. The calcium-silicate-hydrate gel was assessed indirectly via the 20–35° 2θ amorphous hump evolution. For each condition, $n \geq 3$ replicates were tested; results are reported as mean ± SD together with peak positions, full width at half maximum, and refinement residuals.

4. Results and Discussion

4.1. Rheological Properties and Fluidity of Leak-Stopping Cement Slurry

(1) Adjustment of the Water-Cement Ratio for Cement Slurry

The water-to-cement ratio (W/C) is a fundamental parameter governing the rheological properties, fluidity, filtration behavior, and cured structure of cement slurry. In conventional cementing operations, the W/C ratio is typically maintained within 0.44–0.50 to achieve higher cement stone strength and lower permeability. However, under fracture or vugular loss conditions in deep and ultra-deep wells, the performance requirements differ markedly, shifting the focus from "enhancing cementing strength" to "ensuring pumpability and forming a continuous, stable plugging structure". Consequently, lost-circulation control systems often require a relatively higher W/C ratio to improve flow and penetration in complex fracture channels [32–34].

Figure 3 illustrates the rheological behavior of cement slurry at different W/C ratios. Although all slurries exhibit typical shear-thinning behavior, the curve slopes and viscosity levels vary appreciably with changes in the W/C ratio. As the W/C ratio increases from 0.5 to 0.7, the shear stress decreases markedly and the viscosity is reduced, indicating more pronounced thinning behavior. Meanwhile, Figure 4 shows that fluidity increases from approximately 200 mm to 238 mm, reflecting enhanced spreading and diffusion behavior. The on-site flow morphology in Figure 5 further confirms the slurry's excellent pumpability and fracture adaptability.

Considering pumpability, structural stability, and compatibility with subsequent bridging materials, W/C = 0.6 was selected as the base formulation. On the one hand, compared with W/C = 0.5, this system exhibits lower viscosity and improved fluidity, providing enhanced penetration in fractures. On the other hand, compared with W/C = 0.7, it maintains a reasonable solid-skeleton density, supplying essential structural support for particle bridging, fiber reinforcement, and final curing densification. Thus, W/C = 0.6 achieves an optimal balance between rheological performance and structural integrity, making it the most suitable base system for bridging composite lost-circulation slurry.

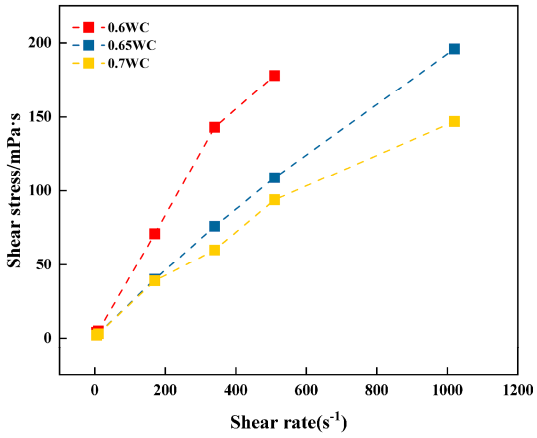


Figure 3. Rheological properties of cement slurry at different water to cement ratios.

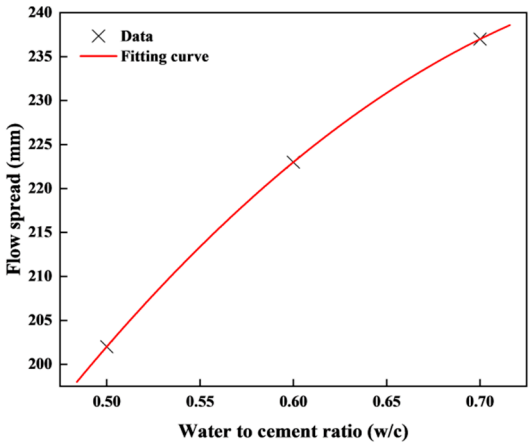


Figure 4. Effect of water to cement ratio on slurry flowability.



Figure 5. Flow behavior of the cement slurry at a water–cement ratio of 0.6.

(2) Adjustment of the Rheological Properties of Cement Slurry by Additive Incorporation

Figure 6 demonstrates that the addition of a dispersant (SP) significantly reduces the shear viscosity and yield stress of the cement slurry. As the SP dosage increases, the plastic viscosity (PV) decreases from approximately 46 mPa·s to about 30 mPa·s, and the yield point (YP) decreases from around 18 Pa to approximately 11–12 Pa. The mechanism lies in the ability of the dispersant to weaken flocculated structures, enhance electrostatic

repulsion and steric hindrance, and shift particles from a flocculated to a dispersed state, thereby producing more pronounced shear-thinning behavior. For plugging, this rheological behavior—characterized by reduced viscosity, decreased yield stress, and easy flow initiation—significantly improves slurry pumpability, reduces pumping pressure, and enhances penetration into fractures and fine channels, thereby laying the foundation for forming a stable plugging structure. Therefore, the primary role of the dispersant is reflected in the "pumping and penetration phase," making it a key regulatory factor for improving plugging efficiency.

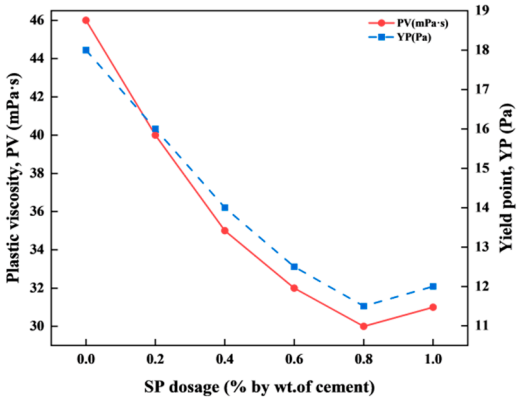


Figure 6. Effect of dispersant dosage on the pumping performance of cement slurry.

In contrast, Figure 7 shows that as the dosage of the fluid-loss reducer (CS) increases, both PV and YP exhibit a clear upward trend, with PV rising from approximately 32 mPa·s to about 40 mPa·s and YP increasing from around 12 Pa to about 16 Pa. This indicates that the fluid-loss reducer strengthens the particle network by forming water-absorbing gels or colloidal protective layers, thereby increasing the structural viscosity of the system. Higher viscosity and yield stress provide greater resistance to water separation, sedimentation, and erosion during the "residence and plugging phase," helping maintain the geometric shape and structural integrity of the plugging layer under high differential pressure. Additionally, good colloidal stability helps maintain the uniform distribution of fibers and particle-bridging materials, thereby preventing plugging failure caused by solid–liquid separation [35]. Therefore, the primary contribution of the fluid-loss reducer lies in improving the structural retention capacity of the slurry, enabling it to reside stably in fractures, gradually densify, and form a reliable plugging skeleton, thereby improving plugging durability under high-temperature and high-pressure downhole conditions.

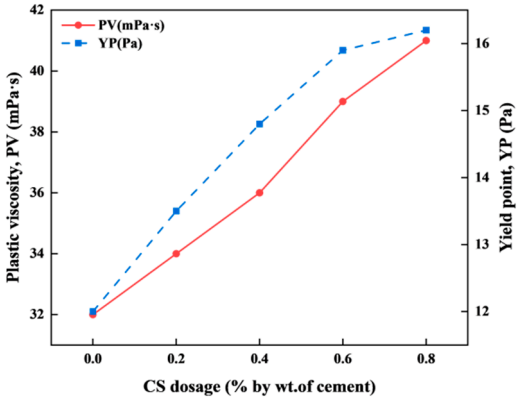


Figure 7. Effect of fluid-loss additive dosage on the structural viscosity of cement slurry.

(3) Effect of Fibers on the Rheological Properties of Cement Slurry

Figure 8 illustrates that different fiber types exhibit significant differences in the pumping performance and thixotropy of cement slurry. Under the same dosage (0.4 wt%), carbon fibers produce the lowest plastic viscosity and the highest structural recovery rate (R60), indicating the most favorable combined pumping and thixotropic performance. Basalt fibers exhibit intermediate viscosity and R60 values, whereas glass fibers markedly increase viscosity and reduce structural recovery, which is detrimental to the balance between pumpability and thixotropy. These differences primarily result from variations in dispersion behavior, stiffness, and surface properties among the fibers, leading to the formation of distinct spatial skeleton structures within the slurry. Carbon fibers, owing to their excellent dispersibility and high stiffness, maintain uniform distribution under shear and promote the formation of a microstructural network. In contrast, glass fibers tend to entangle and agglomerate, disrupting the flow structure, increasing viscosity, and inhibiting thixotropic recovery. Overall, fiber type exerts varying effects on the pumping and static phases of the cement slurry, with carbon fibers providing the most favorable performance balance and thus being more suitable for plugging systems.

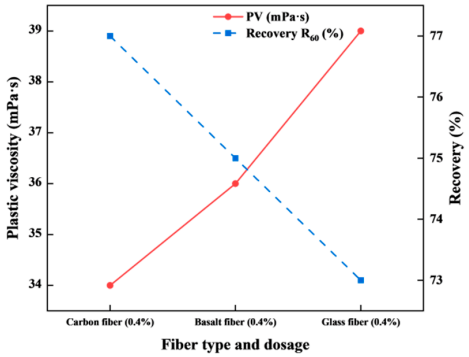


Figure 8. Effect of different fiber types on the pumpability and thixotropy of cement slurry.

Figure 9 indicates that as the carbon-fiber content increases from 0 to 0.6 wt%, the plastic viscosity gradually increases, while the structural recovery rate (R60) initially rises and then stabilizes, reaching an optimal value at approximately 0.4–0.5 wt%. This suggests that an appropriate fiber content can form an effective microscale support network within the slurry, enhancing structural reconstruction after shear failure and facilitating the formation of a stable plugging structure during the static phase. However, excessive fiber content may lead to increased entanglement or local agglomeration, raising flow resistance and reducing thixotropic recovery. Therefore, carbon fibers offer clear advantages in improving thixotropy and structural stability, and the optimal dosage range (0.4–0.5 wt%) achieves the best balance between pumping performance and structural retention, making it the ideal enhancement range for plugging cement slurry.

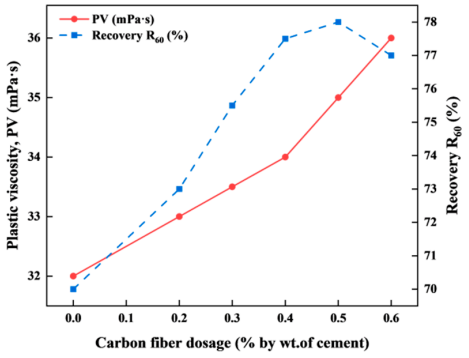


Figure 9. Effect of carbon fiber dosage on the pumpability and thixotropy of cement slurry.

4.2. Assessment of Thickening Behavior in Plugging Cement Slurry

Figure 10 demonstrates that the retarder dosage exerts a significant and sustained delaying effect on the thickening time of the cement slurry. As the retarder concentration increases from 0 to 3.0 wt%, the thickening time extends from approximately 60 min to nearly 300 min, exhibiting a distinct nonlinear growth trend. This indicates that the retarder effectively inhibits the formation rate of early hydration products (particularly C–S–H), weakens particle bridging, and thereby delays the transition of the slurry from a fluid to a gel state [36]. In deep and ultra-deep well plugging environments—characterized by high formation temperatures, long sealing sections, and complex annuli—premature thickening can result in pump sticking or insufficient fracture penetration. Therefore, regulating the retarder dosage is essential to ensure that the system retains an adequate operational window and controllability under high-temperature conditions.

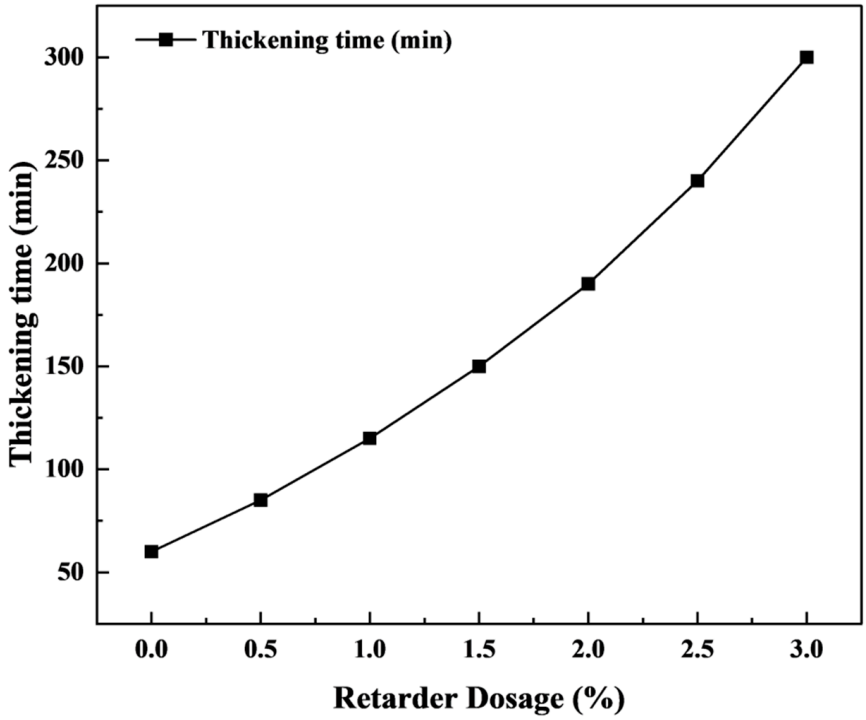


Figure 10. Effect of retarder dosage on the thickening time of cement slurry.

Figure 11 illustrates the thickening evolution of the cement slurry under a 2.5 wt% retarder, further revealing the characteristics of the thickening stage. At approximately 200 °C and 45 MPa, the slurry undergoes a rapid thickening phase within the first 40–50 min, with consistency increasing from about 20 Bc to a stable range of approximately 60 Bc. Subsequently, it maintains a plateau over an extended period, indicating good viscosity stability and continuous pumpability under high-temperature conditions. Finally, a rapid increase in consistency occurs at around 260 min, marking the onset of the nonpumpable stage, i.e., the thickening endpoint. This process highlights that: (i) the retarder significantly extends the pumpable window at high temperatures; (ii) the consistency plateau reflects a stable colloidal structure minimizing water separation and rapid gelation; and (iii) accelerated thickening in the final stage ensures timely solidification after fracture penetration and residence, forming a reliable plugging structure.

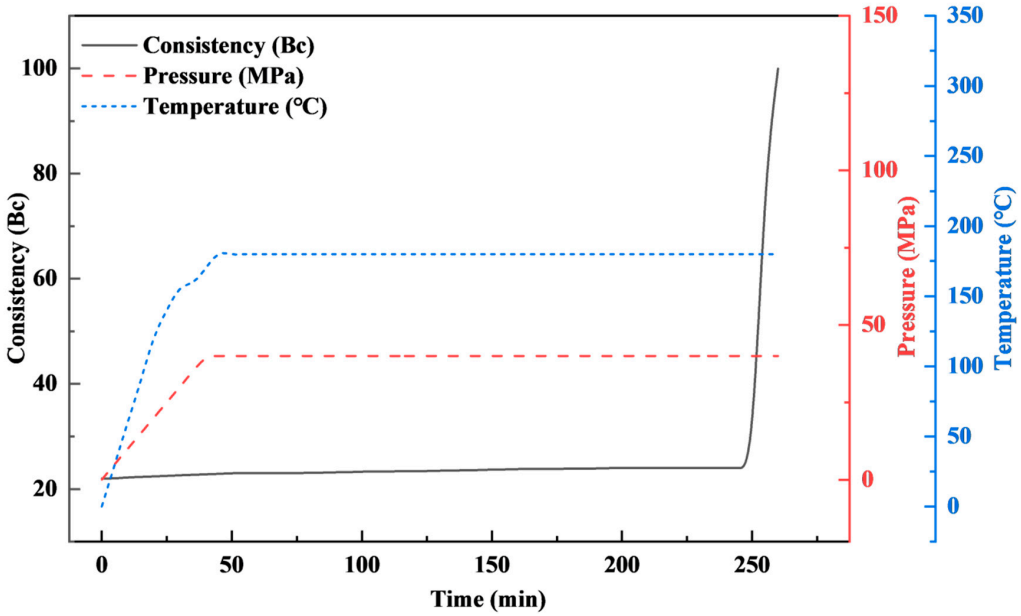


Figure 11. Thickening behavior of cement slurry at a 2.5% retarder dosage.

4.3. Colloidal Stability Evaluation of Plugging Cement Slurries

Figure 12 demonstrates that the incorporation of both nano-SiO_2 and micron-scale SiO_2 significantly reduces the bleeding rate of the cement slurry, with nano-SiO_2 showing the most pronounced improvement. This indicates that fine-particle admixtures play a critical role in enhancing the colloidal stability of cement slurry. Owing to their higher specific surface area and stronger adsorption capacity, nano-scale materials can more effectively bind free water and fill fine pores in the hydration system, thereby forming a denser and more stable colloidal network. In contrast, although micron-scale SiO_2 can also enhance colloidal stability, its larger particle size limits its ability to build early structures and restrain free water. Consequently, nano-SiO_2 provides more pronounced advantages in improving bleeding resistance, anti-settling performance, and overall homogeneity, making it more suitable as a colloidal-stability-enhancing component for cementing slurries.

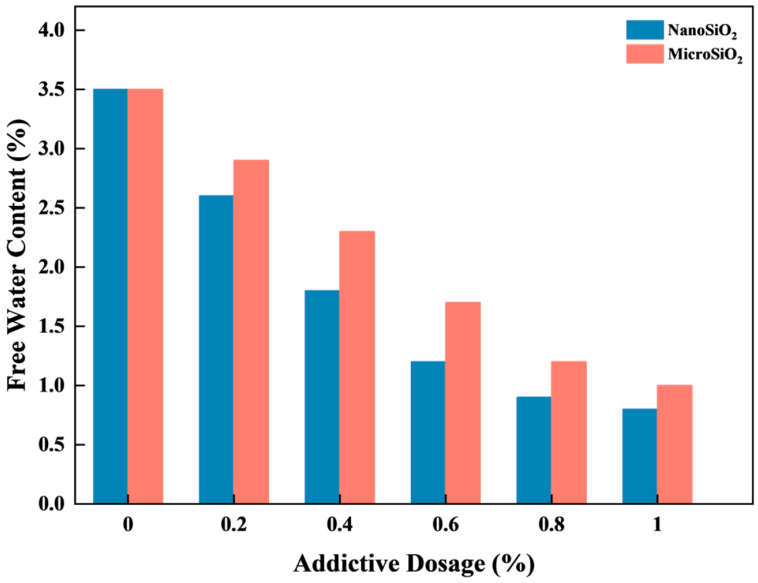


Figure 12. Free water content of cement slurries containing different dosages of Nano-SiO_2 and Micro-SiO_2.

Figure 13 demonstrates that silicon-based stabilizers significantly enhance the colloidal stability of cement slurry. In the control slurry, substantial water separation and distinct stratification interfaces were observed, indicating the poorest suspension stability. Upon the incorporation of microsilica, water separation was markedly reduced and the degree of stratification decreased, although some sedimentation still occurred. In contrast, nano-silica dioxide almost completely inhibited water separation and phase separation, resulting in the formation of a uniform and dense colloidal structure. These findings indicate that nano-SiO_2 exhibits superior performance in enhancing the anti-water separation capability of cement slurry, inhibiting stratification, and improving overall stability, making it the material of choice for optimizing the colloidal stability of deep well plugging cement slurries.

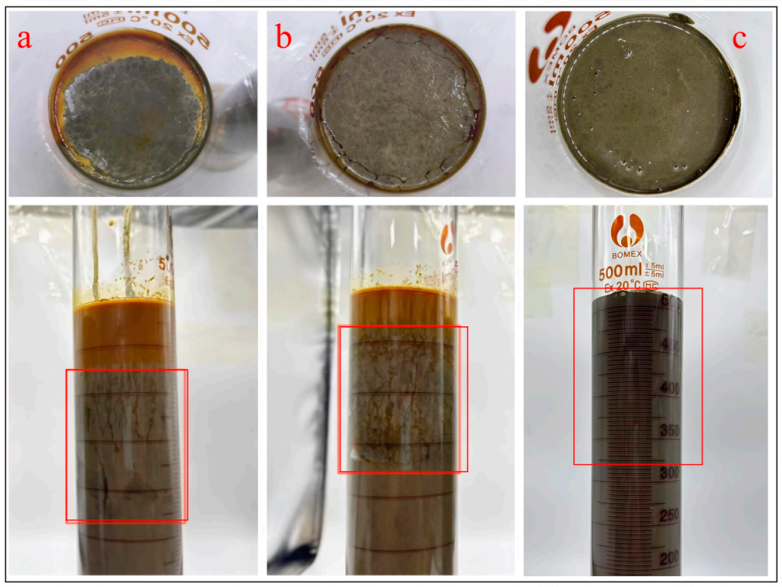


Figure 13. Comparison of bleeding and phase separation characteristics of cement slurries: (**a**) no additive, (**b**) microsilica, and (**c**) nano-SiO_2.

4.4. The Suspension Stability of Cement Slurry on Lost Circulation Materials

To evaluate the suspension stability of cement slurry under varying concentrations of lost-circulation materials (LCMs), this study systematically investigated the density distribution of set cement within an LCM concentration range of 0–20 wt%. By sectioning the set cement along the vertical axis and measuring the density of each segment, the sedimentation tendency of LCMs and the homogeneity of the solidified structure were analyzed. A smaller density variation indicates effective suspension of LCM particles and inhibition of sedimentation stratification during setting, thereby forming a stable and uniform plugging structure. Conversely, a larger density variation suggests insufficient suspension stability, which may result in non-uniform mechanical properties and reduced pressure-bearing capacity of the plugging layer.

Table 2 presents the density distribution across various cement stone segments under different dosages of lost-circulation materials, thereby evaluating the suspension stability of the cement slurry with respect to these materials. Using a 20 wt% dosage as an example, the post-curing density distribution of each segment is illustrated in Figure 11. The density of each segment was calculated according to Equations (4)–(7). By comparing density variations at different heights, the settling tendency of lost-circulation particles during curing and the overall suspension stability of the system can be visually assessed.

$$\rho_1 = \frac{m_1}{v_1} = \frac{197.05}{105} = 1.8589 \quad (4)$$

$$\rho_2 = \frac{m_2}{v_2} = \frac{196.59}{104} = 1.8902 \quad (5)$$

$$\rho_3 = \frac{m_3}{v_3} = \frac{195.97}{102} = 1.9026 \quad (6)$$

$$\rho_4 = \frac{m_4}{v_4} = \frac{195.72}{102} = 1.9188 \quad (7)$$

Table 2. Density Distribution of Cement Stone Segments with Different Leak-Stopping Materials.

Number	Percentage Increase in Leak-Stopping Material (%)	ρ_1 (g·cm^{-3})	ρ_2 (g·cm^{-3})	ρ_3 (g·cm^{-3})	ρ_4 (g·cm^{-3})	$\Delta\rho = \rho_4 - \rho_1$ (g·cm^{-3})	$G\rho = \Delta\rho/\rho \times 100$ (%)
1	0	1.8400	1.8480	1.8550	1.8600	0.0200	1.09
2	10	1.8500	1.8680	1.8830	1.8900	0.0400	2.16
3	15	1.8550	1.8800	1.8950	1.9050	0.0500	2.70
4	20	1.8589	1.8902	1.9026	1.9188	0.0599	3.22

From an overall trend perspective, as the dosage of leak-stopping material increases from 0% to 20%, the density of each cement stone segment progressively increases, indicating that high-density leak-stopping particles enhance the overall solid content of the system and lead to a more compact solidified structure [37]. Concurrently, the density difference Δρ increases with dosage, rising from 0.0200 g·cm^{-3} at 0% to 0.0599 g·cm^{-3} at 20%, while the corresponding relative density difference Gρ increases from 1.09% to 3.22%. This suggests that at higher dosages, a certain degree of particle sedimentation occurs, but the density difference remains within a reasonable range of approximately 3%, with no significant stratified solidification observed, indicating that overall suspension stability is well maintained.

Figure 14 presents the density measurements for the sample with a 20% dosage. The solidified columnar cement stone was divided into four segments along the height direction, with densities from bottom to top of 1.8589, 1.8902, 1.9026, and 1.9188 g·cm^{-3}, respectively, indicating a slight "heavier-at-the-top and lighter-at-the-bottom" distribution. This is attributed to the good suspension capability of fine particles and nano-fillers in the leak-stopping material during the slurry rheological process, allowing them to remain relatively uniformly dispersed before solidification, thereby reducing overall sedimentation and ensuring structural uniformity.

In summary, the addition of leak-stopping material does not cause significant stratified solidification. Even at a high dosage of 20%, the system maintains high colloidal stability and a uniform spatial structural distribution. This structural uniformity is crucial for crack sealing, as it enables the formation of a continuous, dense, and strength-balanced sealing body, laying the foundation for high bearing-pressure performance and stable sealing capacity.

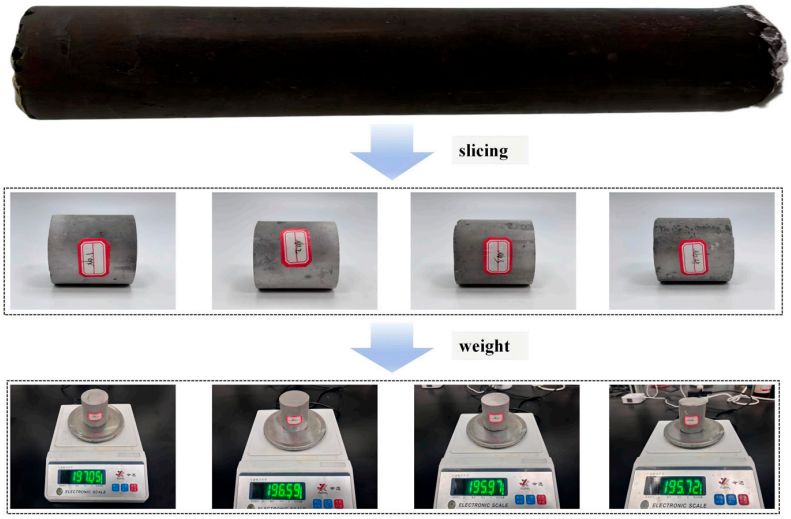


Figure 14. Density distribution of different sections of the cured cement slurry with 20% LCM content.

4.5. Experimental Evaluation of Fracture-Sealing Performance

4.5.1. Bridge-Building Pressure During the Sealing Process

Figures 15 and 16 demonstrate that the bridging composite lost-circulation slurry undergoes four distinct phases—initial flow, bridge formation, thickening enhancement, and stable sealing—in both 1.5 mm and 3 mm fractures, ultimately achieving effective sealing. However, significant differences are observed in the sealing-establishment rate and structural density between the two fracture scales. In 1.5 mm fractures, bridging is completed within 2–4 min, with pressure rapidly increasing to approximately 4.0 MPa and stabilizing, while leakage simultaneously decreases to nearly zero, indicating that the slurry readily remains in place and rapidly forms a dense sealing layer. In contrast, in 3 mm fractures, bridging initiation is delayed to approximately 6–7 min, with a more gradual pressure increase and a notably prolonged leakage-decay phase. Nevertheless, the system can progressively establish a stable sealing structure through continuous thickening and compaction, ultimately achieving a pressure-bearing capacity of approximately 3.8 MPa.

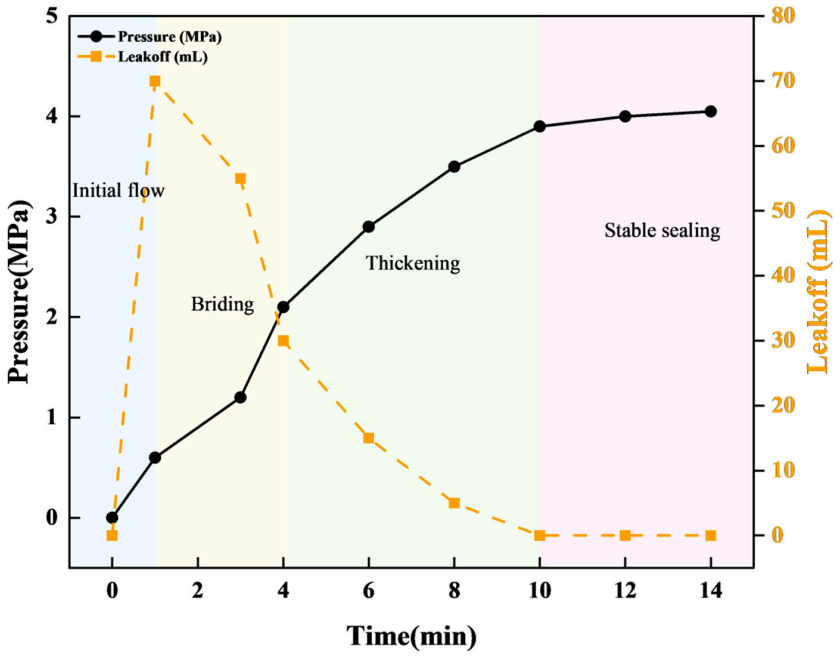


Figure 15. Pressure development and leakoff evolution of cement slurry during bridge formation in a 1.5 mm fracture.

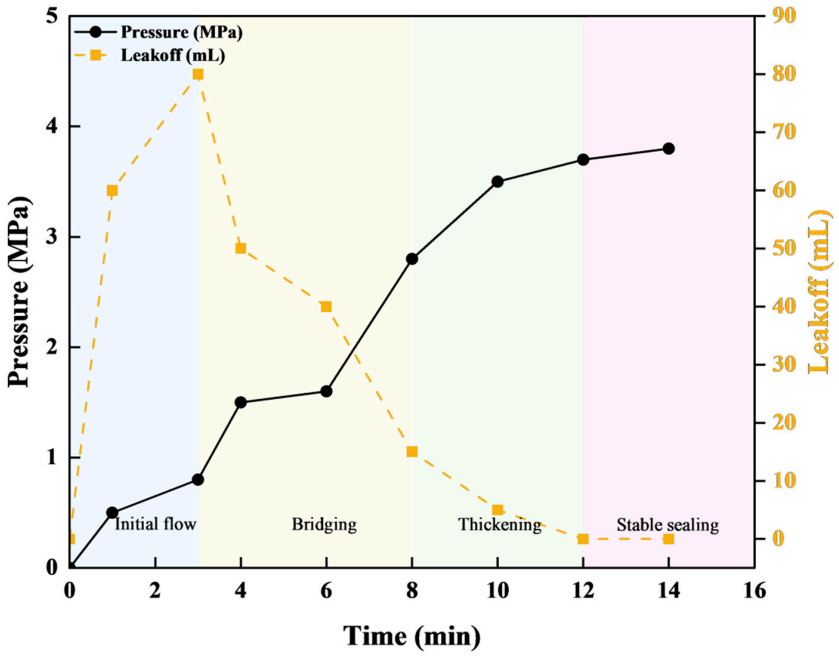


Figure 16. Pressure development and leakoff evolution of cement slurry during bridge formation in a 3 mm fracture.

The cross-sectional structure of the sealing layer shown in Figure 17 further corroborates these observations. Regardless of fracture width, the lost-circulation slurry can construct a continuous three-dimensional framework composed of cement matrix, particles, and fibers. The sealing body in 1.5 mm fractures is denser and more uniform, whereas in 3 mm fractures, although localized weak zones exist, the overall sealing layer maintains good continuity and adhesion. This indicates that the composite lost-circulation system can adapt to different fracture scales and form reliable sealing structures, although the sealing-formation rate and final density decrease as fracture width increases.

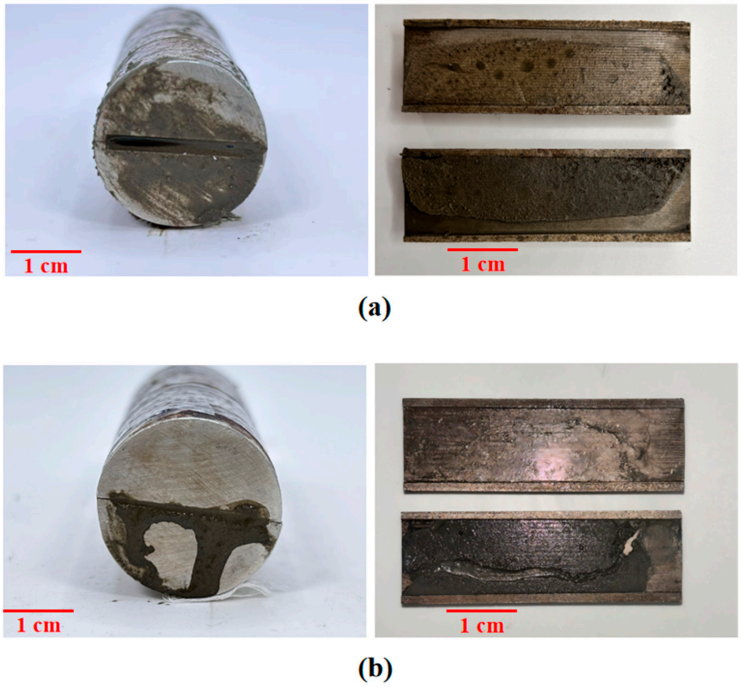


Figure 17. Steel fracture model and the internal structure of the sealing layer, (**a**) 3 mm fracture; (**b**) 1.5 mm fracture.

4.5.2. Compressive-Bearing Capacity of the Solidified Sealant

Compared with conventional particle- or fiber-dominant temporary plugging methods that primarily rely on short-term bridging, the proposed cement-based composite system is designed to form an integrated sealing body after setting. Therefore, the expected performance emphasizes post-setting integrity and high-temperature pressure-bearing stability, which is critical for fracture-induced losses in deep and ultra-deep wells.

Figure 18 demonstrates that the cured cement plug maintains considerable compressive strength across a range of aging temperatures, although it exhibits a gradual decrease in strength as temperature increases. At 25 °C, the plug reaches its peak compressive strength of approximately 16 MPa. When the aging temperature increases to 120–150 °C, the compressive strength undergoes a slight reduction but remains within 13–14 MPa. With a further increase to 180 °C, the compressive strength decreases to approximately 12 MPa, which still meets the mechanical load-bearing requirements for deep-fracture sealing. These results indicate that the cement plugging system retains excellent structural integrity and mechanical stability under high-temperature conditions.

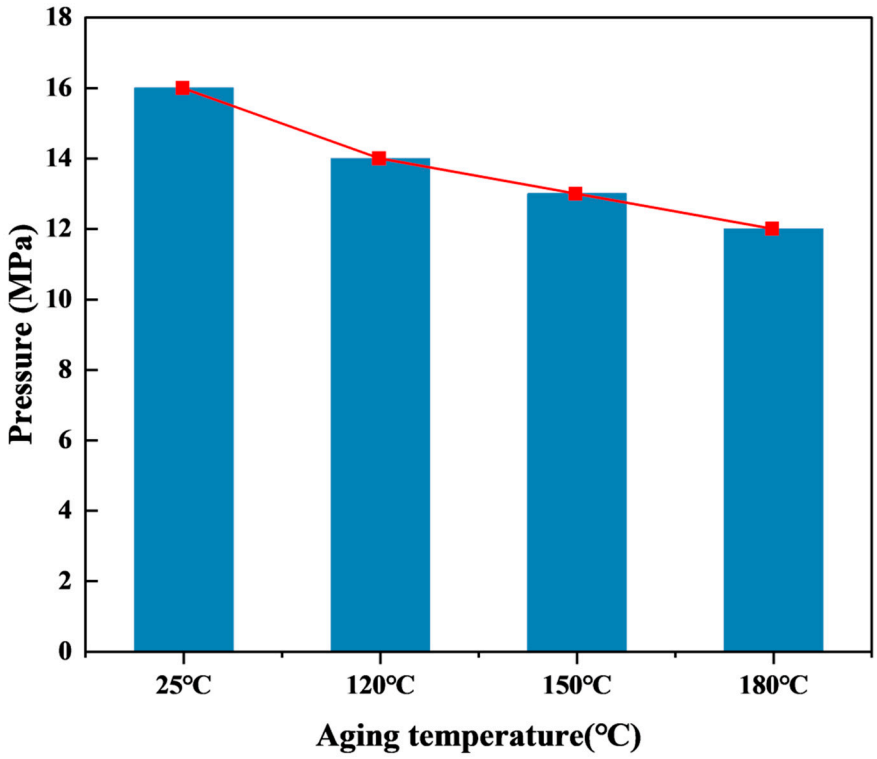


Figure 18. Pressure-bearing performance of the cement plug formed inside the fracture (The red curve represents the variation trend of the pressure-bearing capacity of the sealing body).

4.5.3. Sealing Integrity of the Solidified Sealant

The experimental results demonstrate that the cured cement-based sealing material maintains high pressure-bearing and sealing capacity under varying temperature conditions when tested in a water medium, indicating excellent interfacial adhesion and bonding strength. As illustrated in Figure 19, even under high-temperature aging at 150–180 °C, the sealing material exhibits no significant interfacial degradation or structural delamination, thereby maintaining stable sealing pressure. This confirms that the formed cementitious sealing structure possesses superior interfacial bonding stability and resistance to thermal damage in high-temperature environments, effectively blocking fluid migration and forming a durable, reliable sealing barrier. These findings highlight that the sealing system not only exhibits excellent high-temperature pressure-bearing capacity but also demonstrates

outstanding interfacial bonding and long-term sealing stability, meeting the stringent performance requirements for sealing materials in the harsh downhole environments of deep fractured formations.

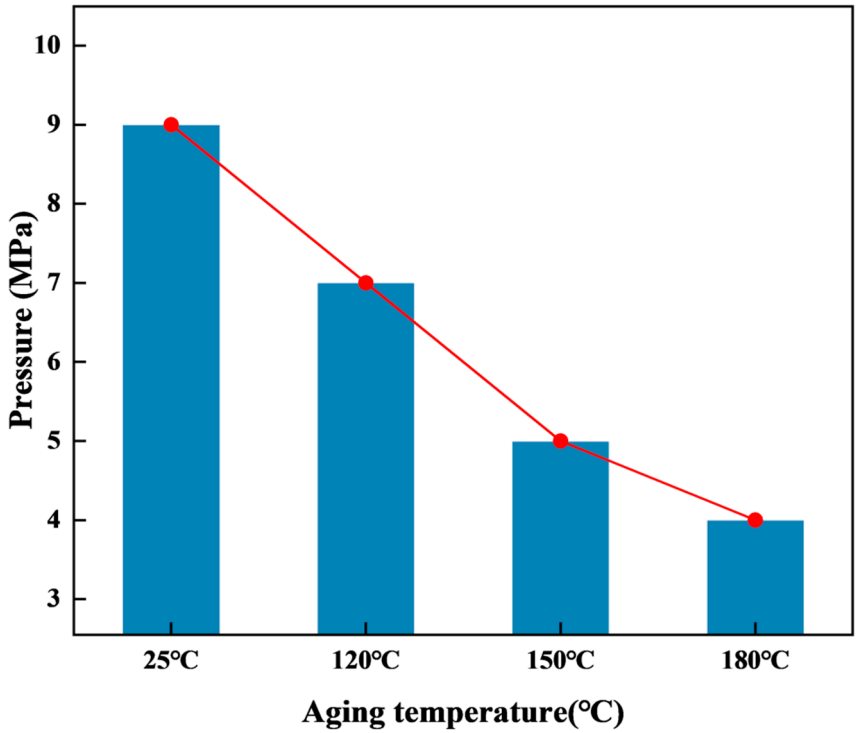


Figure 19. Sealing performance of the cement-based plug inside the fracture (The red curve represents the variation trend of the pressure-bearing capacity of the sealing body).

4.5.4. Comparison of the Composite Bridging Plugging System with Other Systems

According to Table 3, under the condition of 1.5 mm rigid cracks, there are significant differences in retention ability, sealing performance and pressure-bearing capacity among the various formulations of cement slurry. The base slurry system exhibits typical instability and loss behavior, unable to establish a sealing pressure. Pure cement slurry lacks rapid bridging and accumulation of a framework, continuously leaking under pressure difference and erosion, and is difficult to remain. The crack channel remains unobstructed, and gas migration is not blocked, resulting in continuous gas migration and inability to form a subsequent load-bearing structure.

Even after adding 0.5% fibers to the base slurry, it still shows "total leakage and gas migration", indicating that relying solely on fiber network bridging is insufficient to resist erosion and shear damage within the crack. When there is a lack of particle framework support, fibers are more likely to form local flexible entanglements, making it difficult to form a stable blocking core and the continuous channel still cannot be cut off.

When 20% blocking particles are added to the base slurry, the system transitions from failure to effective sealing, with a sealing performance after curing reaching 2 MPa. This indicates that the particles can bridge at the crack opening and form an accumulation framework, significantly enhancing the retention ability and initially blocking the channel. However, it performs poorly in the sealing and curing pressure-bearing tests. There are still seepage channels or weak interfaces within the plugged layer, resulting in limited tightness and anti-seepage ability. Under high pressure difference, liquid seepage or re-compression may occur.

Table 3. Summary of the comparison of sealing capabilities between the composite bridge plug system and other systems.

Serial Number	Crack Size	Formula	Sealing Result	Plugging Performance Before Curing/MPa		Sealing Performance After Curing/MPa		Plugging Performance After Curing/MPa	
1	1.5 mm	Base Slurry	Failure to Seal	/	Complete Leakage, Gas Migration	/	/	/	/
2	1.5 mm	Base Slurry + 0.5% Fiber	Failure to Seal	/	Complete Leakage, Gas Migration	/	/	/	/
3	1.5 mm	Base Slurry + 20% Leak-Stopper Particles	Successful Sealing	2	Leakage Stopped, Gas Migration Disappeared	4	Flowing Liquid	8	Flowing Liquid
4	1.5 mm	Base Slurry + 0.5% Fiber + 20% Leak-Stopper Particles	Successful Sealing	4	Leakage Stopped, Gas Migration Disappeared	8	Flowing Liquid	15	Flowing Liquid

The combined system's plugging performance before curing is increased to 4 MPa, indicating that a more stable bridging and accumulation structure can be formed during the unsealing stage, with better retention ability than the particle-only system. The sealing performance after curing is improved to 8 MPa, indicating that the synergy of fibers and particles significantly reduces pore connectivity and enhances the continuity of the sealing band, thereby improving anti-seepage and pressure-bearing capabilities. The plugging performance after curing reaches 15 MPa before liquid seepage occurs, indicating that it maintains structural stability under higher pressure and has the best overall performance.

Building on prior research, Wang et al. developed a high-temperature/high-pressure (HTHP) resin-based lost-circulation material that achieves an effective sealing pressure of 10 MPa for fracture widths of 1–3 mm [38]. Addressing fracture-induced losses, Xu et al. formulated an oil-based drilling-fluid plugging system with a pressure-bearing capacity exceeding 7 MPa for fractures narrower than 3 mm [39]. Through synergistic compounding of multi-component lost-circulation materials, Kang et al. further increased the sealing pressure to 13 MPa [40]. In comparison, the proposed high-temperature bridging composite system not only achieves a post-set pressure-bearing capacity above 13 MPa, but also exhibits superior high-temperature stability, enabling adaptation to harsher downhole thermal environments. Overall, this system offers pronounced technical advantages for high-temperature, high-pressure drilling in deep and ultra-deep wells.

4.6. Mechanical Properties of Cement Stone

4.6.1. Analysis of the Compressive Strength of Cement Stone

Figure 20 illustrates the mechanical response curves and failure patterns of cement stone under three distinct formulation conditions, clearly demonstrating the influence of fibers and plugging particles on its load-bearing performance and toughness. For the reference cement stone without additives (Figure 20a), the peak load is relatively low, and the failure mode is characterized by brittle fracture, with extensive spalling and penetrating cracks observed on the specimen surface. This indicates that ordinary cement stone lacks effective crack-blunting mechanisms during loading, making it prone to sudden failure.

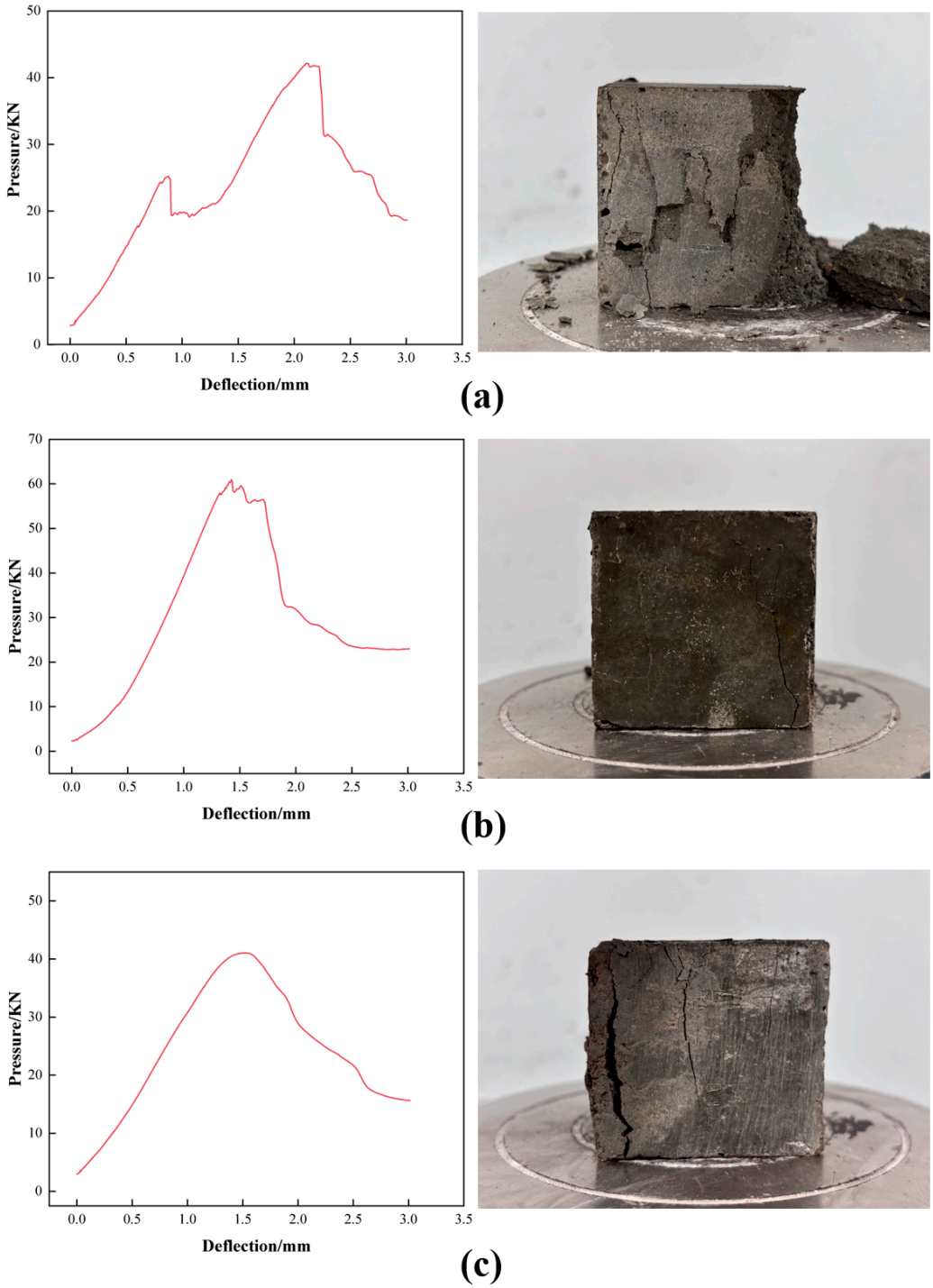


Figure 20. Mechanical performance curves of the cement plug under different formulations ((**a**): no additives; (**b**): 0.5% fiber; (**c**): 20% LCM + 0.5% fiber).

With the incorporation of 0.5% fibers (Figure 20b), the peak load-bearing capacity of the cement stone significantly increases, and the descending segment of the curve becomes more gradual, reflecting improved toughness and energy-absorption capability. The fibers form a three-dimensional bridging structure within the cement matrix, constraining crack propagation and delaying failure during loading, thereby enhancing the overall integrity of the specimen. In this case, failure is primarily localized to edge cracks.

For the composite system incorporating 20% plugging particles and 0.5% fibers (Figure 20c), the peak strength is slightly lower than that of the fiber-only sample, but the load-bearing curve is more robust, exhibiting a distinct plastic stage before failure. This

indicates enhanced compressive strength and sealing stability of the system. The three-dimensional reinforcement framework synergistically formed by the plugging particles and fibers enhances structural uniformity and strain-coordination capability, allowing the specimen to maintain residual strength even in the later failure stages. The corresponding failure mode is characterized primarily by non-penetrating cracks, resulting in a more stable overall structure.

4.6.2. Analysis of the Cement Stone's Bonding Strength

Table 4 presents the tensile bonding strength of cement stone for three formulations. The base cement slurry exhibits a maximum destructive force of 16.71 kN (Figure 21a), corresponding to a bonding strength of 0.99 MPa, indicating a relatively limited interface bearing capacity primarily governed by cement hydration products. With the incorporation of 0.5% fibers, the maximum force increases to 22.11 kN (Figure 21b), and the bonding strength to 1.30 MPa, representing an increase of approximately 32% compared with the base slurry. Further addition of 20% leak stopper particles leads to a maximum destructive force of 29.59 kN (Figure 21c), and a bonding strength of 1.74 MPa, which is about 77% higher than that of the base slurry and 34% higher than that of the fiber-reinforced system. The increase in bonding strength can be attributed to enhanced mechanical interlocking and improved stress distribution at the interface.

Table 4. The cement stone's bonding strength under different formulations.

Serial Number	Formula	Maximum Force/KN	Section Area/m^2	Gluing Strength/MPa
1	Basic Cement Slurry	16.71452	0.0169646	0.985258901
2	Basic Cement Slurry + 0.5% Fiber	22.10975	0.0169646	1.30328768
3	Basic Cement Slurry + 0.5% Fiber + 20% Leak-Stopper Particles	29.58727	0.0169646	1.744059723

4.7. XRD Analysis of Cement Stone

Figure 22 presents the XRD patterns of set cement obtained from an LCM-containing slurry cured at 90 °C, 180 °C, and 200 °C. The characteristic portlandite reflection at $2\theta \approx 18.1^\circ$ and the diffraction responses at 29.4–29.6°, 32.2–32.4°, and 34.1–34.3° occur at invariant 2θ positions with only minor intensity fluctuations; changes in peak position and FWHM lie within instrumental/sample-preparation uncertainty, with no additional reflections and no disappearance of major peaks. Together with the near-absence of clinker reflections (C_3S, C_2S) and the stable amorphous hump of C–S–H at 20–35°, these results indicate that the specimens are essentially fully hydrated across the tested temperatures. The lack of deleterious secondary phases, along with stable/narrowing peak shapes, is consistent with a compact microstructure. No systematic peak shift or new peak appears after adding LCM, confirming chemical compatibility and no detectable interference with hydration or densification.

4.8. SEM Analysis of Cement Stone Microstructure

Scanning electron microscopy (SEM) images (Figure 23) reveal that conventional cement slurry (a, b) exhibits a loose and porous internal structure, characterized by weak interparticle bonding and the absence of continuous, stable support networks, resulting in poor structural homogeneity. In contrast, the composite bridging plugging cement slurry (c, d) exhibits a markedly different microstructural morphology. With the synergistic incorporation of fibers, particles, and flake materials, a three-dimensional support

framework is gradually formed, creating a denser and more uniform structure with enhanced spatial continuity. The fibers span pores and connect particles, functioning at the microscale to "bridge, toughen, and stabilize the framework," thereby inhibiting microcrack initiation and propagation and enhancing microstructural integrity. Overall, the dense three-dimensional framework formed by the composite plugging system is markedly superior to that of conventional cement stone, enhancing erosion resistance, structural toughness, and pressure-bearing stability, and providing a robust microscopic foundation for forming a high-strength, long-term stable sealing layer in fractures.

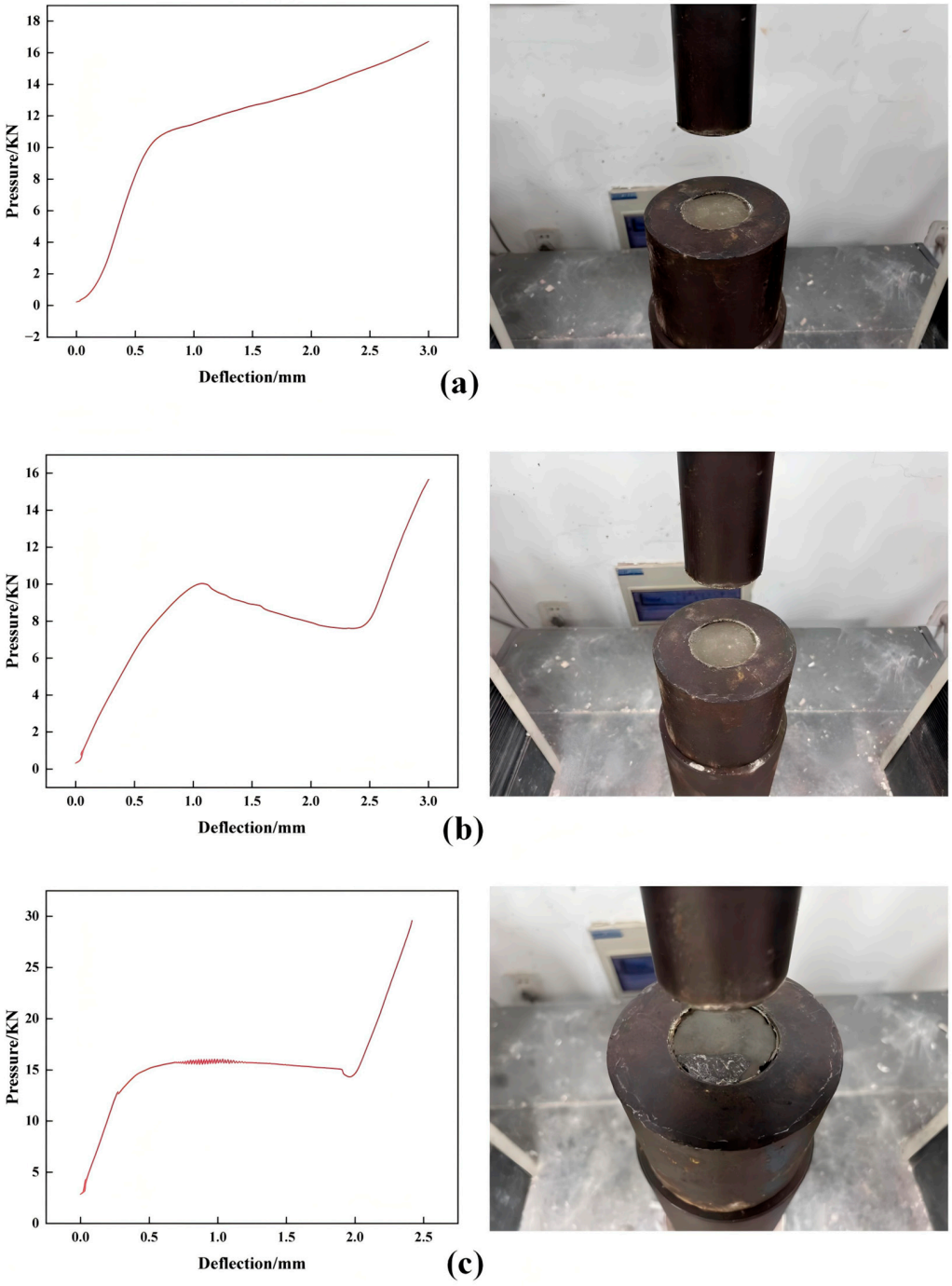


Figure 21. The cement plug's bonding strength curves under different formulations ((**a**): without additives; (**b**): 0.5% fibers; (**c**): 20% LCM + 0.5% fibers).

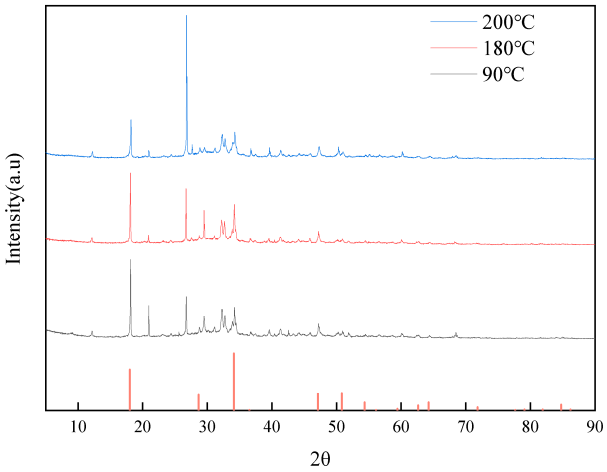


Figure 22. XRD spectra of LCM-containing cement stone at different temperatures, The orange lines indicate the characteristic diffraction peaks of $Ca(OH)_2$.

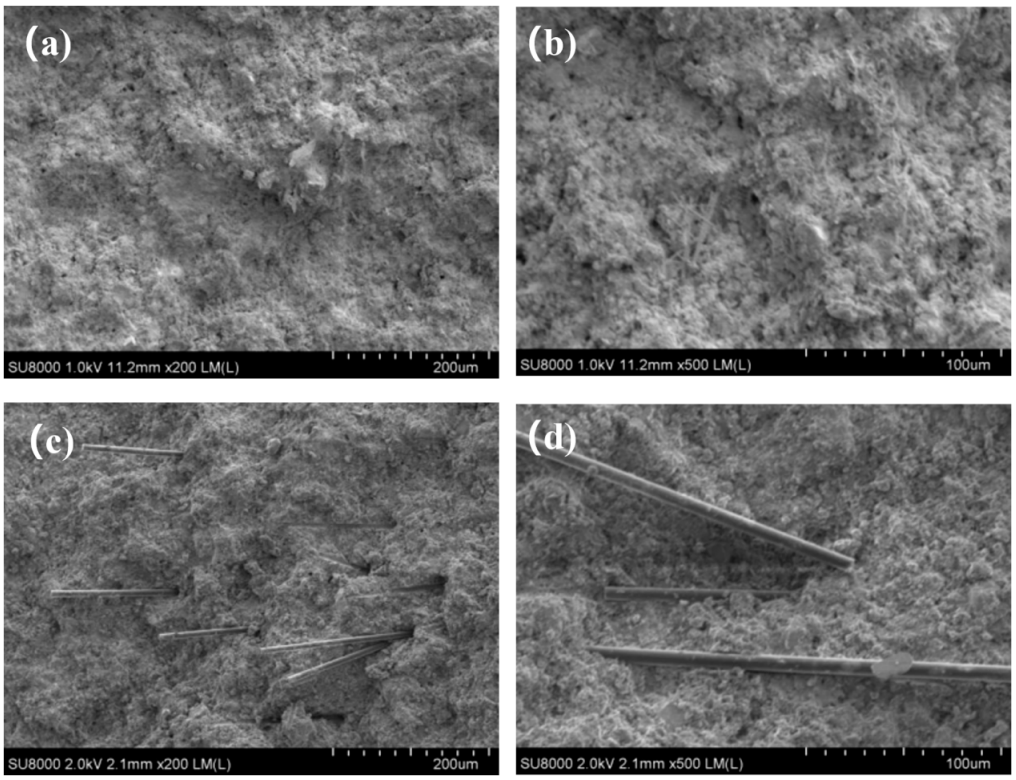


Figure 23. Microscopic images of the cement-based slurry at different magnifications ((**a**): 200×; (**b**): 500×) and the composite bridging–plugging cement slurry ((**c**): 200×; (**d**): 500×).

5. Conclusions

This study systematically evaluated a composite bridging plugging cement slurry for deep and ultra-deep fractured formations. The main findings are as follows:

(1) A W/C ratio of 0.6 provides a practical balance between pumpability and fracture retention, and the combined use of dispersant and fluid-loss reducer improves slurry stability and suspension performance.

(2) The incorporation of nano-SiO_2, microsilica, and fibers effectively suppresses segregation and bleeding, with the cured density variation controlled within 3%.

(3) The slurry achieves reliable sealing in both 1.5 mm and 3 mm fractures, forming a stable plugging structure after placement and curing.

(4) Under 25–180 °C, the cured plugging body maintains effective integrity, with the pressure-bearing capacity decreasing from 16 MPa to ~12 MPa while the sealing capacity remains from 9 MPa to ~4 MPa.

Overall, the proposed system demonstrates stable rheology, high-temperature performance retention, and fracture-plugging capability, supporting its potential for high-temperature loss-circulation control in deep fractured formations.

Author Contributions: Conceptualization, B.M. and K.Z.; methodology, B.M.; software, B.F. and S.Z.; validation, K.Z.; formal analysis, Q.S.; investigation, Q.S.; resources, Q.S.; data curation, L.P.; writing—original draft preparation, P.X.; writing—review and editing, C.Z.; visualization, Z.Z.; supervision, Z.Z. and S.Z.; project administration, S.Z.; funding acquisition, L.P. All authors have read and agreed to the published version of the manuscript.

Funding: This research was supported by the CNPC Chuanqing Drilling Engineering Company Limited Science and Technology Project "Development of a 200 °C-Resistant Cement-Based Plugging System for Deep-Well Lost Circulation Control" (CQ2024B-4-Z2-3); PetroChina Company Limited Science and Technology Project "Integrated Research and Field Testing of Safe and Efficient Drilling and Completion Technologies for Deep Formations in Western Sichuan" (2024ZS49).

Data Availability Statement: The original contributions presented in this study are included in the article. Further inquiries can be directed to the corresponding authors.

Acknowledgments: We would like to thank The Bakken Laboratory of YANGTZE University for their support.

Conflicts of Interest: Authors Biao Ma, Kun Zheng, Bin Feng, Qing Shi, Chengjin Zhang were employed by the company Downhole Service Company of CNPC Chuanqing Drilling Engineering Company Limited. Authors Zhengguo Zhao was employed by the company Drilling Fluid Company of CNPC Chuanqing Drilling Engineering Company Limited. The remaining authors declare that the research was conducted in the absence of any commercial or financial relationships that could be construed as a potential conflict of interest.

References

1. Amani, M. HPHT 101-What Petroleum Engineers and Geoscientists Should Know About High Pressure High Temperature Wells Environment. *Energy Sci. Technol.* **2012**, *4*, 36–60. [CrossRef]
2. El Sabeh, K.; Gaurina-Međimurec, N.; Mijić, P.; Medved, I.; Pašić, B. Extended-Reach Drilling (ERD)—The Main Problems and Current Achievements. *Appl. Sci.* **2023**, *13*, 4112. [CrossRef]
3. Elkatatny, S.; Ahmed, A.; Abughaban, M.; Patil, S. Deep Illustration for Loss of Circulation While Drilling. *Arab. J. Sci. Eng.* **2020**, *45*, 483–499. [CrossRef]
4. National Bureau of Statistics of China. *Deep Exploration Trend Report*; National Bureau of Statistics of China: Beijing, China, 2022.
5. Magzoub, M.I.; Salehi, S.; Hussein, I.A.; Nasser, M.S. Loss Circulation in Drilling and Well Construction: The Significance of Applications of Crosslinked Polymers in Wellbore Strengthening: A Review. *J. Pet. Sci. Eng.* **2020**, *185*, 106653. [CrossRef]
6. Zhong, L.; Zhang, J.; Zhong, S.; Li, H. Well integrity threats caused by severe losses. *Nat. Gas. Ind. B* **2020**, *6*, 347–355.
7. Sinopec. *Deep Sichuan Basin Drilling Geological Report (Internal Dataset)*; Sinopec: Beijing, China, 2023.
8. Sun, J.; Bai, Y.; Cheng, R.; Lyu, K.; Liu, F.; Feng, J.; Lei, S.; Zhang, J.; Hao, H. Research progress and prospect of plugging technologies for fractured formation with severe lost circulation. *Pet. Explor. Dev.* **2021**, *48*, 732–743. [CrossRef]
9. PetroChina Drilling Institute. *HPHT Well Failure Investigation Report*; PetroChina Drilling Institute: Beijing, China, 2022.
10. Abdollahpour, P.; Moradi, S.S.T.; Leusheva, E.; Morenov, V. Stress-cage and fracture closure modeling. *Energies* **2022**, *15*, 5439. [CrossRef]
11. Alsaba, M.; Al-Dushaishi, M.; Nygaard, R. Updated PSD criterion for LCM. *J. Pet. Sci. Eng.* **2017**, *149*, 641–648. [CrossRef]
12. Scott, P.; Redburn, M.; Nesheim, G. A Pragmatic Approach to Lost Circulation Treatments: What Every Drilling Engineer Should Know. In Proceedings of the AADE Fluid Conference, Houston, TX, USA, 14–15 April 2020; pp. 14–15.
13. Nygaard, R.; Hareland, G.; Alsaba, M.T.; Contreras, O.; Alsaba, M. Assessment of LCM particle-size vs sealing. *Drill. Complet.* **2017**, *37*, 191–201.

14. Kibikas, W.; Nakagawa, S.; Ingraham, M.; Bauer, S.; Chang, C.; Dobson, P.; Kneafsey, T.; Samuel, A. Thermal degradation effects on LCM sealing. *Energies* **2024**, *17*, 2703. [CrossRef]
15. Lei, S.; Sun, J.; Bai, Y.; Lv, K.; Zhang, S.; Liu, F.; Zhang, J. Plugging Performance and Mechanism of Temperature-Responsive Adhesive Lost Circulation Material. *J. Pet. Sci. Eng.* **2022**, *217*, 110771. [CrossRef]
16. Zhou, C.; Hu, D.; Wehling, C. Degradation of Particulate LCM, the Thermal Influence. In Proceedings of the AADE National Technical Conference and Exhibition, Hilton Denver City Center, Denver, CO, USA, 9–10 April 2019.
17. Alqutt, M.; Sabaa, A.; Elshamy, H. Cognitive Bias in Well Integrity Investigations: A Case Study on Casing Leaks in Egypt's Western Desert. In *Proceedings of the Abu Dhabi International Petroleum Exhibition and Conference, Abu Dhabi, United Arab Emirates, 3–6 November 2025*; SPE: Abu Dhabi, United Arab Emirates, 2025; p. D021S040R006.
18. Fidan, E.; Babadagli, T. *Cement as LCM—Field application*; SPE Asia Pacific: Mid Valley City, Malaysia, 2004.
19. Effectiveness of High-Performance Water-Based Spacer Systems for Curing Lost Circulation in Permeable Reservoirs During Cementing Operations | SPE Nigeria Annual International Conference and Exhibition | OnePetro. Available online: https://onepetro.org/SPENAIC/proceedings-abstract/17NAIC/17NAIC/195521 (accessed on 13 January 2026).
20. Innovative and Established LCM Cementing Solutions Combined to Create Novel LCM Cementing Fluid Train | SPE Norway Subsurface Conference | OnePetro. Available online: https://onepetro.org/SPEBERG/proceedings-abstract/19BERG/19BERG/D011S005R002/217448 (accessed on 13 January 2026).
21. Tan, H.; Shen, L.; Zuo, Y.; Fan, L.; Zhang, G.; Qiu, D.; Xie, L.; Zheng, X.; He, W. Light-Weight Temporary-Sealing Cement for Medium Temperature Geothermal Wells by Using Polyvinyl Alcohol Fibers and Fly Ash Cenospheres. *J. Pet. Sci. Eng.* **2022**, *215*, 110704. [CrossRef]
22. Yang, Y. Evaluation methodology for cement-based LCM. *Chem. Eng. Res. Des.* **2018**, *136*, 348–358.
23. Zhu, M.F.; Yang, H.H. Polypropylene fibers. In *Handbook of Fiber Chemistry*; Springer: Dordrecht, The Netherlands, 2007; Chapter 3.
24. Arachchige, W.N.B. Aging and Long-Term Performance of Elastomers for Utilization in Harsh Environments. Ph.D. Thesis, Montan University Leoben, Leoben, Austria, 2019.
25. Chen, X.; Wang, C.; Xue, Y.; Chen, Z.; Jin, J.; Wang, R. A Novel Thermo-Thickening Viscosity Modifying Admixture to Improve Settlement Stability of Cement Slurry under High Temperatures. *Constr. Build. Mater.* **2021**, *295*, 123606. [CrossRef]
26. Wang, Q.; Zhu, Q.; Shao, T.; Yu, X.; Xu, S.; Zhang, J.; Kang, Q. The rheological test and application research of glass fiber cement slurry based on plugging mechanism of dynamic water grouting. *Constr. Build. Mater.* **2018**, *189*, 119–130. [CrossRef]
27. Gaurina-Međimurec, N.; Pašić, B.; Mijić, P.; Medved, I. Drilling fluid and cement slurry design for naturally fractured reservoirs. *Appl. Sci.* **2021**, *11*, 767. [CrossRef]
28. *GB/T 8077-2012*; Methods for Testing Uniformity of Concrete Admixture. National Standard: Beijing, China, 2012.
29. *GB/T 19139-2012*; Testing of Well Cements. National Standard: Beijing, China, 2012.
30. Feng, J.; Zheng, L.; Wu, X.; Wu, J.; Yu, Y.; Li, L.; Li, M. Preparation and characterization of polymer retarder for plugging cement slurry. *J. Dispers. Sci. Technol.* **2023**, *44*, 2239–2246. [CrossRef]
31. Su, Q.; Jiang, X.; Yin, H.; Ma, X.; Zhao, J.; Yuhuan, B.; Guo, S.; Liu, H. Research and Evaluation of a Plugging System with Integrated Cementing and Bridging Properties. In Proceedings of the ISOPE International Ocean and Polar Engineering Conference, Rhodes, Greece, 16–21 June 2024.
32. Liu, S.; Peng, B.; Liu, J.; Wang, M.; Li, G. Research on the diffusion plugging mechanism of flowing water grouting slurry in karst pipelines. *Sci. Rep.* **2024**, *14*, 19246. [CrossRef]
33. Blinov, P.A.; Salakhov, K.N.; Nikishin, V.V.; Kuchin, V.N. Development of Cement Slurry Composition with Self-healing Properties. *Int. J. Eng.* **2025**, *38*, 236–246. [CrossRef]
34. Syed, H. Best practices in designing HP/HT cement-plug systems. In *Proceedings of the SPE Annual Technical Conference and Exhibition, Denver, CO, USA, 21–24 September 2008*; SPE: Richardson, TX, USA, 2008.
35. Mesaud, R.; Shafqat, A.; Al-Jadhar, A.; Kharchi, S.; Bermudez, F.; Pohl, J. Challenging Plug & Abandon Cementing Operation under Influx and Losses Scenario. In *Proceedings of the Mediterranean Offshore Conference, Alexandria, Egypt, 20–22 October 2024*; SPE: Richardson, TX, USA, 2024.
36. Roye, J.; Sam, P. Don't Get Stung Setting Balanced Cement Plugs: A Look at Current Industry Practices for Placing Cement Plugs in a Wellbore Using a Stinger or Tail Pipe. In *Proceedings of the SPE/IADC Drilling Conference and Exhibition, Fort Worth, TX, USA, 4–6 March 2014*; SPE: Richardson, TX, USA, 2014.
37. Vogl, A.; Waldal, N.; Sarmadi, P.; Fershtman, A.; Mitishita, R.; Frigaard, L.A. Plug cementing stability. In *Proceedings of the International Conference on Offshore Mechanics and Arctic Engineering, Hamburg, Germany, 5–10 June 2022*; American Society of Mechanical Engineers: New York, NY, USA, 2022; Volume 85956.
38. Wang, C.; Zhang, Z.; Wang, T.; Fu, K.; Xie, G. High-Pressure- and High-Temperature-Resistant Resins as Leakage Control Materials in Drilling Fluids. *Processes* **2025**, *13*, 1353. [CrossRef]

39. Shu, M.; Zhao, M.; Xu, M. Plugging while Drilling Technology Using Oil-Based Drilling Fluid in Fuling Shale Gas Field. *Pet. Drill. Tech.* **2017**, *45*, 21–26.
40. Kang, Y.; Yu, H.; Xu, C.; Tang, L. An Optimal Design for Millimeter-Wide Facture Plugging Zone. *Nat. Gas Ind. B* **2015**, *2*, 113–119. [CrossRef]

Disclaimer/Publisher's Note: The statements, opinions and data contained in all publications are solely those of the individual author(s) and contributor(s) and not of MDPI and/or the editor(s). MDPI and/or the editor(s) disclaim responsibility for any injury to people or property resulting from any ideas, methods, instructions or products referred to in the content.